THE JOURNAL OF PHYSICAL CHEMISTRY C

Article

pubs.acs.org/JPCC

Ultra-Antireflective Electrodeposited Plasmonic and PEDOT Nanocone Array Surfaces

Han Wai Millie Fung, Seulgi So, Kellen Kartub, Gabriel Loget,† and Robert M. Corn*

Department of Chemistry and Department of Biomedical Engineering, University of California−Irvine, Irvine, California 92697, United States

Supporting Information

ABSTRACT: Novel broadband ultra-antireflective surfaces were created via the electrodeposition of a nanostructured zinc oxide thin film onto conductive, light absorbing periodic nanocone arrays. Nanocone arrays of (i) fluorinated ethylene propylene (FEP) coated with a 50 nm plasmonic gold thin film and (ii) the electroactive polymer poly(3,4-ethylenedioxythiophene) (PEDOT) exhibited a very low broadband reflectivity of less than 0.1% from 475 to 800 nm at a wide range of incident angles after the electrodeposition of a nanostructured ZnO thin film onto the surface. SEM images reveal the formation of ZnO nanoflowers and nanorods on both nanocone array surfaces; these additional ZnO nanostructures enhance the coupling of the incident visible light into the absorptive gold or PEDOT nanocones to significantly reduce the reflectivity of these surfaces. The ZnO-coated nanocone array surfaces also exhibited an enhanced photoreactivity for the oxidative degradation of methylene blue, suggesting their potential to be used as a self-cleaning antireflective surface.

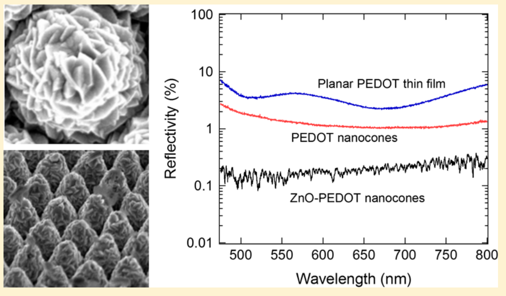

■ INTRODUCTION

Nanostructured array surfaces can provide excellent broadband antireflectivity over a wide range of optical wavelengths and incident angles and have been incorporated as optical coatings into various devices such as solar cells,[1,2] photodetectors,[3] and electroreflective windows.[4] Traditionally, arrays of transparent zinc oxide nanostructures have been fabricated by chemical vapor deposition[5−7] or electrochemical methods[8−11] to create a graded interfacial refractive index coating that increases the transmittance of silicon solar cell devices by reducing the reflectivity of the device surface down to approximately 2−5%.[12−14] However, when a transparent nanostructured ZnO coating is used in a hierarchical fashion with a subwavelength periodic array of an absorbing material,[15,16] an even better broadband antireflective surface can be created. Recently, we have demonstrated the fabrication of periodic absorptive nanocone arrays of gold-coated fluorinated ethylene propylene (FEP)[17] and the electroactive polymer poly(3,4-ethylenedioxythiophene) (PEDOT);[18] our large area fabrication process employs the oxygen plasma etching of a square centimeter scale polymer substrate or thin film that has been covered with a colloidal monolayer of polystyrene (PS) beads. The resultant plasmonic gold and PEDOT nanocone array surfaces both exhibited excellent broadband antireflectivity; for the gold surfaces, a reflectivity of less than 1% was observed from 475 to 800 nm over a wide range of incident angles.[17] In this article, we show that the reflectivity for both the gold and PEDOT nanocone arrays can be reduced even further by the electrodeposition of a nanostructured ZnO coating; for the PEDOT nanocone arrays, up to a 10-fold reduction in reflectivity is observed with the surface being 0.1% to 0.2% reflective from 475 to 800 nm while transmitting from 2% to 10% in the same spectral region. In addition, we demonstrate that the antireflective nature of the ZnO-coated nanocone arrays can be explained using 11-phase Fresnel calculations to model the graded refractive index and absorption changes at the air/nanocone interface. To the best of our knowledge, no one has fabricated surfaces with lower reflectivities than our broadband ultra-antireflective ZnO nanostructured surfaces. The ultra-antireflective ZnO-coated nanocone array surfaces are characterized with scanning electron microscopy (SEM), X-ray diffraction (XRD), and X-ray photoelectron spectroscopy (XPS) and additionally are shown to be photocatalytic with potential as self-cleaning surfaces. Moreover, the PEDOT nanocone arrays are electroreflective and thus can be incorporated into electro-optical devices.[18] These ultra-antireflective surfaces are extremely useful in applications where reflections must be absolutely minimized; examples include laser optics[19,20] and antiglare coatings for mirrors displays, cameras, and lenses.[21,22]

■ EXPERIMENTAL METHODS

Fabrication of FEP−Au Nanocone Array Surfaces. A FEP substrate with a 0.005″ thickness (CS Hyde Company) was cleaned by rinsing with ethanol and Milli-Q water followed by O_2 plasma cleaning (PDC-32G, Harrick Plasma) for 3 min.

Received: July 28, 2017
Revised: September 14, 2017
Published: September 15, 2017

DOI: 10.1021/acs.jpcc.7b07503
J. Phys. Chem. C 2017, 121, 22377−22383

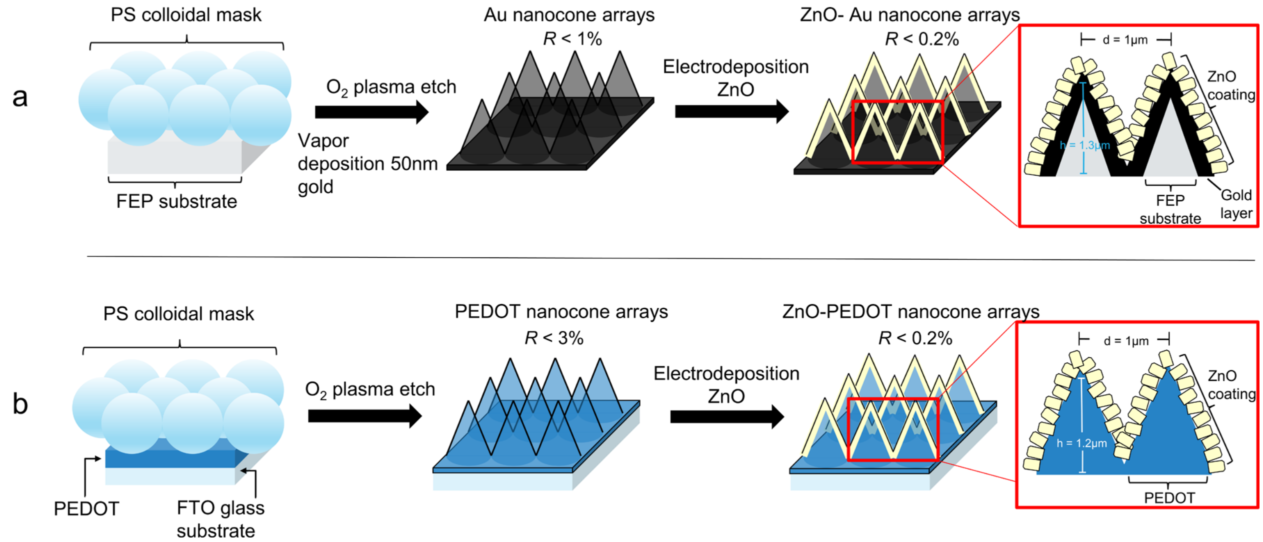

Figure 1. Schematic illustration of the fabrication of ultra-antireflective ZnO-coated nanocone arrays using (a) FEP-Au nanocone arrays and (b) PEDOT nanocone arrays.

A solution of PS beads with a diameter of 1 μm (Polyscience Polybead carboxylate, 2.6% w/v) was centrifuged and transferred to a mixture containing ethanol and methanol in a 2:1 ratio with 0.2% volume of TX-100 surfactant, adjusted to a PS concentration of about 5%. To form the PS colloidal mask monolayer, the PS beads were spin-coated onto the FEP substrate at 650 rpm for 15 s, followed by 1200 rpm for 0.5 s, then left at room temperature for a few minutes to dry the solvent. The PS bead/FEP substrate was then etched by O_2 plasma for 6 min to form periodic FEP nanocone arrays. The FEP nanocone arrays were finally coated with 50 nm of gold by thermal evaporation.

Fabrication of PEDOT Thin Film. A fluorine-doped tin oxide coated glass slide substrate (FTO-glass; ~30 Ω/sq, Sigma-Aldrich) was cleaned by sonication in a 0.2% volume aqueous TX-100 solution, followed by sonication in ethanol, then dried under a nitrogen stream, and finally cleaned by O_2 plasma cleaning (PDC-32G, Harrick Plasma) for 3 min. A layer of PEDOT:PSS (2.0 wt % in H_2O, high conductivity grade, Sigma-Aldrich) was spin-coated at 2000 rpm for 45 s onto the FTO substrate to improve wetting and conductivity. The sample was dried for 20 min in a 90 °C oven. PEDOT thin film was then deposited electrochemically onto the FTO substrate using an aqueous plating solution consisting of 2.5 mM EDOT (97%, Sigma-Aldrich) and 12.5 mM $LiClO_4$ (99.5%, Alfa) via cyclic voltammetry. The electrodeposition was performed using a potentiostat (Metrohm Autolab PGSTAT12) sweeping from 1.045 to 0.9 V at 0.01 V/s for 10 cycles, with a Ag/AgCl reference electrode and a Pt counter electrode.

Fabrication of PEDOT Nanocone Array Surfaces. A solution of PS beads with a diameter of 1 μm (Polyscience Polybead carboxylate, 2.6% w/v) was centrifuged and transferred to a mixture containing ethanol and methanol in a 2:1 ratio with 0.2% volume of TX-100 surfactant, adjusted to a PS concentration of about 5%. To form the PS colloidal mask monolayer, the PS beads were spin-coated onto the PEDOT film at 750 rpm for 15 s, followed by 1200 rpm for 0.5 s, then left at room temperature for a few minutes to dry the solvent. The PS bead/PEDOT sample was then etched by O_2 plasma for 2.5 min to form periodic PEDOT nanocone arrays.

Fabrication of ZnO-Coated Nanocone Array Surfaces. An aqueous solution of 0.1 M $Zn(NO_3)_2{\cdot}6H_2O$ (98%, Sigma-Aldrich) at pH 4 heated to 70 °C was used as the plating solution. Electrodeposition was performed using a potentiostat (PGSTAT12, Metrohm) in a three-electrode setup. The working electrode of either Au or PEDOT nanocone array surfaces was exposed to the plating solution for 150 s at a cathodic potential of −0.9 V against a Ag/AgCl reference electrode and in the presence of a Pt counter electrode.

Characterization. SEM images were obtained on a FEI Magellan 400 field-emission scanning electron microscope at an accelerating voltage of 5 kV. Grazing incidence XRD measurements were performed on a Rigaku SmartLab X-ray Diffractometer, with the X-ray generator operating at 40 kV and 44 mA with Cu Kα irradiation. XPS measurements were performed using a Kratos Analytical AXIS Supra surface analysis instrument at an emission current of 15 mA. For reflectivity and transmittance measurements, a halogen lamp was used as a white light source (10 V, B&K Precision DC regulated power supply). The emitted white light was coupled to an optical fiber (Thorlabs M25L01), collimated using an achromatic lens (f = 50 mm, Thorlabs AC254-050-A-ML), then made incident to the sample surface. The reflected or transmitted light from the sample surface is coupled to an optical fiber (Ocean Optics P1000-2-VIS/NIR) with an achromatic lens (f = 30 mm, Thorlabs AC254-030-A-ML), then measured with a UV−vis−NIR spectrometer (Ocean Optics USB4000). Reflectivity measurements were calibrated with a silver mirror reference, whereas transmittance measurements were calibrated using air as reference.

Photocatalytic Degradation of Methylene Blue. One milliliter of a 50 μM aqueous methylene blue (MB) solution and a 1 cm^2 photocatalytic surface (either ZnO-coated nanocone arrays or planar ZnO thin film) were added in a quartz cuvette. The cuvette was exposed to a UV lamp source (50 W, Oriel Instruments Hg(Xe) arc lamp) while stirring to ensure contact between the ZnO surface and the MB. The relative concentration of MB remaining was determined after the following time intervals: 0, 2, 4, 6, 8, 10, 12, and 14 min. Relative MB concentrations were determined from the absorbance measurement at λ = 664 nm using UV−vis

DOI: 10.1021/acs.jpcc.7b07503
J. Phys. Chem. C 2017, 121, 22377−22383

spectroscopy (Hewlett-Packard 8453 UV−visible spectrometer).

■ RESULTS AND DISCUSSION

Large scale periodic ZnO-coated nanocone array surfaces (areas on the order of square cm) were fabricated using a combination of colloidal lithography, plasma etching, vapor deposition, and electrochemistry. As shown in the scheme in Figure 1, the simultaneous oxygen plasma etching of a hexagonally closed packed monolayer of PS bead colloidal mask spin-coated onto either a FEP substrate or a PEDOT thin film created periodic nanocone arrays; nanocone formation occurs due to the simultaneous etching of both the PS colloidal mask and the polymer underneath. The aspect ratio of the resultant nanocones can be optimized: the size of the PS beads controls the distance between the nanocones, while the O_2 plasma etching time controls the height of the nanocones. In this article, PS beads with a 1 μm diameter were used as the colloidal mask. In the next step, the FEP nanocone arrays were made conductive via vapor deposition of a 50 nm layer of gold, whereas the PEDOT nanocone arrays were already conductive. Finally, an additional nanostructured ZnO coating was created using electrochemistry. In this approach, 0.1 M aqueous zinc nitrate ($Zn(NO_3)_2$) at pH 4.0 was used as the plating solution, and electrodeposition occurred at 70 °C for 150 s at an cathodic potential of −0.9 V against a Ag/AgCl reference electrode. The mechanism of the ZnO electrodeposition process is described as follows: At a sufficiently negative applied potential, NO_3^- ions are reduced to generate OH^- ions (eqn 1). The OH^- and the Zn^{2+} ions then result in the precipitation of ZnO onto the Au or PEDOT nanocone array working electrode (eqn 2).[8−11]

$$NO_3^- + H_2O + 2e^- \rightarrow NO_2^- + 2OH^- \quad (1)$$

$$Zn^{2+} + 2OH^- \rightarrow ZnO\downarrow + H_2O \quad (2)$$

Nanostructured polycrystalline ZnO films were formed directly from this facile electrodeposition method, without the need for a subsequent thermal annealing step. The electrodeposition process was monitored by chronoamperometry of the working electrode (either the Au or PEDOT nanocone arrays), as shown in Supporting Information Figure S1. The initial increase and the subsequent gradual decrease of the absolute current density over time indicated that the conductive nanocone array surfaces became slightly passivated with the addition of a ZnO thin film.

The morphology of the ZnO-coated nanocone arrays was characterized using a combination of SEM, XRD, and XPS. SEM images from Figures 2 and 3 show top-down and tilted views of the nanostructured ZnO thin film on Au and PEDOT nanocone arrays, respectively. From Figures 2a,c and 3a,c, it can be seen that hexagonally close packed ZnO-coated nanocones were created on a large scale, extending over an area of several square microns. Comparing the heights of the ZnO-coated nanocones with Au and PEDOT nanocones from Figures 2d and 3d, respectively, using SEM measurements, we determined that a 25 nm of ZnO coating was formed during electrodeposition. Figures 2b and 3b showed a high magnification image of an individual ZnO-coated Au and PEDOT nanocone, respectively, where we could see the individual ZnO nanostructures formed on the surface. XRD analysis (see Supporting Information Figure S2) revealed a polycrystalline wurtzite crystal structure that grew primarily in the ⟨002⟩ direction, which is consistent with previous work in ZnO electrodeposition.[9,10] We also confirmed that ZnO was formed on both the Au and PEDOT nanocone array surfaces via XPS (see Supporting Information Figure S3).

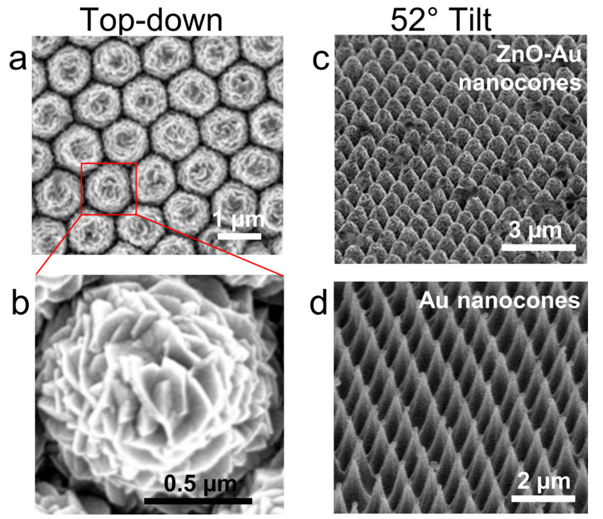

Figure 2. SEM images of ZnO−Au nanocone arrays from top-down (a,b) and tilted (c) views. (d) SEM image of Au nanocone arrays is shown for comparison.

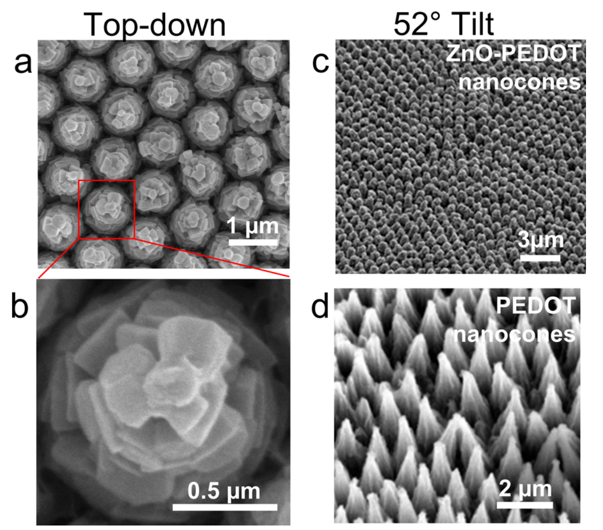

Figure 3. SEM images of ZnO-PEDOT nanocone arrays from top-down (a,b) and tilted (c) views. (d) SEM image of PEDOT nanocone arrays is shown for comparison.

Additionally, the photocatalytic activity of the ZnO-coated nanocone arrays was also characterized via the oxidative degradation of a methylene blue (MB) dye under UV conditions. As shown in Supporting Information Figure S4a, we evaluated the relative concentration of MB over time using UV−vis spectroscopy under the following catalytic conditions: exposure to a ZnO-coated nanocone array surface, planar ZnO thin film surface, and no catalyst. As shown in Supporting Information Figure S4b, 11 ± 1% of the MB remained in solution after 14 min of exposure to a planar ZnO thin film surface, whereas 0 ± 1% of the MB remained in solution after 14 min of exposure to a ZnO-coated nanocone array surface. It should be noted that the planar ZnO thin film surface used in this study is microscopically much smoother than the ZnO-coated nanocone array surface, as shown by the comparison of

DOI: 10.1021/acs.jpcc.7b07503
J. Phys. Chem. C 2017, 121, 22377−22383

their SEM images in Supporting Information Figure S4c,d. For the planar ZnO thin film, the ZnO crystals are packed tightly in the ⟨002⟩ direction,[9,10] which drastically reduces the surface roughness factor compared to the periodic ZnO-coated nanocone arrays. This demonstrates that, since the high surface area of the ZnO-coated nanocone arrays allowed for increased UV absorption,[23,24] the ZnO-coated nanocone array surface performed better as a photocatalyst compared to a planar ZnO thin film surface during MB degradation and may find applications as self-cleaning surfaces.

Optical characterization revealed that the ZnO-coated nanocone array surfaces became more light absorbing and more antireflective than just Au and PEDOT nanocone arrays over a wide range of optical wavelengths from 475 to 800 nm. In Figure 4, the percent transmittance measurements of the ZnO-coated nanocone arrays compared to just Au and PEDOT nanocone arrays are shown. For all transmittance measurements, a halogen lamp was used as a white light source. The light was directed onto the nanocone array surface at a normal angle of incidence, and the transmitted light from the nanocone array surface was measured using a UV−vis spectrometer. As shown in Figure 4a, the transmittance measurements of the Au nanocone arrays were T = 10% or less across the 475 to 800 nm spectral range, indicating strong light absorption. However, the transmittance measurements of the ZnO−Au nanocone arrays were T = 3% in the same spectral range, indicating up to a three-fold improvement in the light absorbing ability of the Au nanocone arrays when they are decorated with ZnO nanostructures on the surface. Similarly, the transmittance measurements for the PEDOT nanocone arrays were T = 10% across the 475 to 800 nm spectral range, but decrease to T = 2% for the ZnO−PEDOT nanocone arrays from λ = 650 to 800 nm, indicating up to a five-fold improvement in the light absorbing ability of the ZnO−PEDOT nanocone arrays across a wide range of optical wavelengths. A possible explanation for the increased light absorbance of the ZnO-coated nanocone arrays is that the ZnO nanostructures on the surface are acting as optical couplers. Although ZnO itself does not absorb in the 475 to 800 nm wavelength range, the ZnO nanostructures on the nanocone array surfaces act as subwavelength scattering components that result in the increased effective optical path length of incident light via coupling and trapping freely propagating plane waves between the ZnO nanostructures and the light absorbing material underneath (either Au or PEDOT). Thus, the nanostructured ZnO surface enhances the light trapping capacity of the nanocone arrays and increases their effective absorption bands.[25−27]

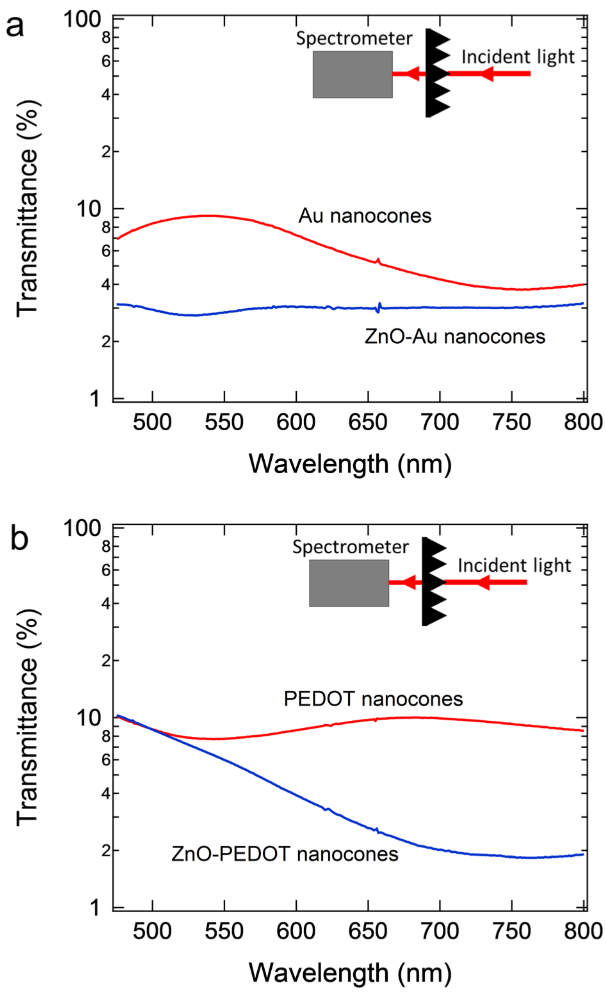

Figure 4. Transmittance spectra for (a) Au and ZnO−Au nanocone arrays and (b) PEDOT and ZnO−PEDOT nanocone arrays. The decrease in transmittance for the ZnO-coated nanocone arrays indicates the ZnO enhances the performance of the light absorbing material underneath (Au or PEDOT). The inserted schematic shows the optical setup used for transmittance measurements.

The most striking effect of the addition of a nanostructured ZnO thin film onto the nanocone arrays was a significant increase in broadband antireflectivity of these surfaces. In our previous papers, we fabricated Au nanocone array surfaces that are less than 0.7% reflective (R < 0.7%) at a nearly normal angle of incidence (θ = 8°) from λ = 475 to 800 nm,[17] and we also recently fabricated PEDOT nanocone array surfaces that were less than 3% reflective (R < 3%) over the same wavelength range.[18] The antireflective behavior of the ZnO-coated nanocone arrays are shown in Figures 5 and 6. For the reflectivity measurements, the optical setup with a halogen lamp white light source at angle of incidence θ = 8°, 45°, or 67.5° was used as shown in the inset of Figure 5, and a silver mirror was used as reference calibration. In Figure 5a, reflectivity measurements are shown for ZnO−Au nanocones in comparison to Au and FEP nanocone arrays at θ = 8°. The FEP nanocone arrays, visually matte white as seen in the photograph from Figure 5b, exhibited broadband antireflective properties at 2% reflective (R = 2%) from λ = 475 to 800 nm. The addition of a 50 nm light absorbing gold thin film on the FEP nanocone arrays created a visually dark Au nanocone array surface (photograph shown in Figure 5c); the percent reflectivity decreased to R < 0.7% over the same spectral range, as seen in Figure 5a. Electrodeposition of a nanostructured ZnO film created ZnO−Au nanocone arrays that were visually even blacker than the Au nanocone arrays (Figure 5c), and the reflectivity measurements for the ZnO−Au nanocone arrays were reduced to R < 0.3% from 450 to 750 nm, with R_{min} = 0.05%. We attribute the very low reflectivity exhibited by the ZnO−Au nanocone array surfaces to increased light scattering by the ZnO nanostructures, as well as an enhancement in the graded interfacial complex refractive index created by the addition of the nanostructured ZnO film to the nanocones.[28−31] To better understand the mechanism responsible for the ultra-antireflective property of the ZnO nanocone arrays, we performed 11-phase Fresnel calculations to model the graded refractive index and absorption changes at

DOI: 10.1021/acs.jpcc.7b07503
J. Phys. Chem. C 2017, 121, 22377−22383

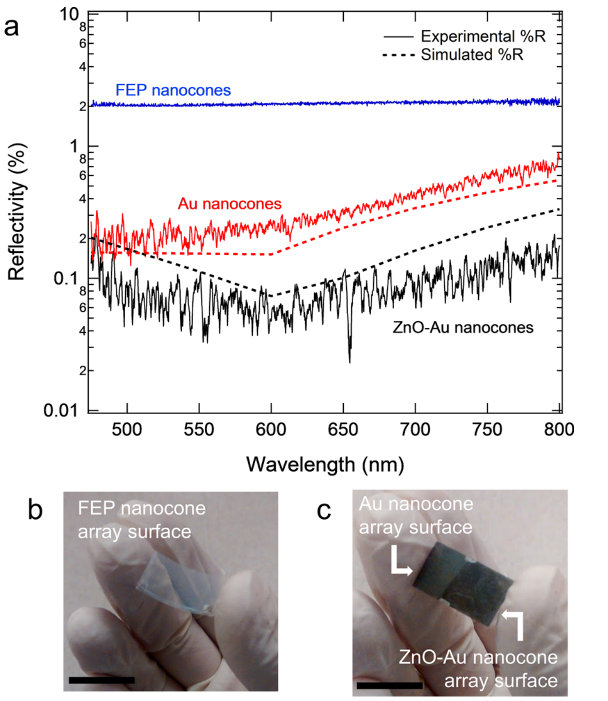

Figure 5. (a) Reflectivity spectra for various nanocone array structures composed of a FEP substrate. Reflectivity measurements are shown for incident light hitting the nanocone array surfaces at a nearly normal angle of incidence (θ) at 8°. Simulated reflectivity measurements obtained from 11-phase Fresnel calculations are also shown for Au and ZnO−Au nanocone arrays. The simulated and experimental reflectivity measurements match well and reveal that ZnO−Au nanocone array surfaces exhibit enhanced antireflective properties. Photographs of (b) FEP nanocone array surface as well as (c) Au and ZnO−Au nanocone array surfaces are shown. The scale bars on the lower left-hand corners represent 1 cm.

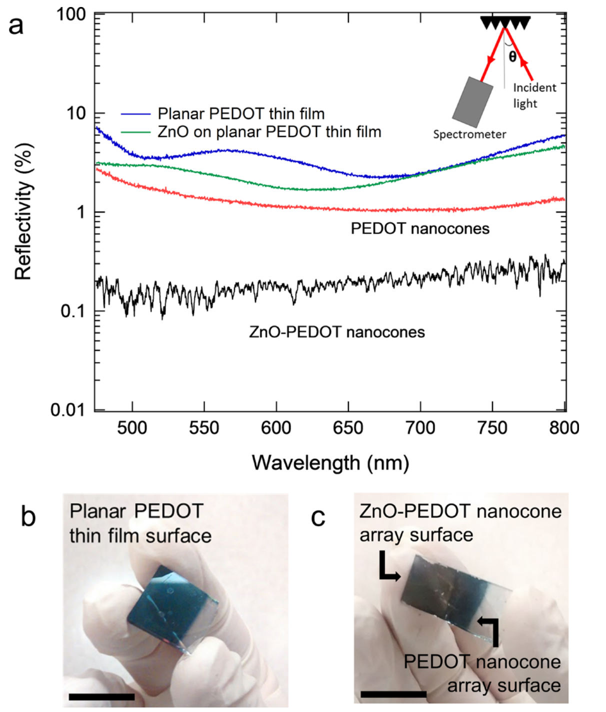

Figure 6. Reflectivity spectra for various nanocone array structures composed of a PEDOT substrate. The ZnO−PEDOT nanocone array surfaces exhibit enhanced antireflective properties. The inserted schematic shows optical setup used for reflectivity measurements. Reflectivity measurements are shown for incident light hitting the surfaces at a nearly normal angle of incidence (θ) at 8°. Photographs of (b) a planar PEDOT thin film surface as well as (c) PEDOT and ZnO−PEDOT nanocone array surfaces are shown. The scale bars on the lower left-hand corners represent 1 cm.

the air/nanocone interface[32] (n_1 = air, n_{11} = bulk Au or ZnO−Au, and n_2, n_3, ..., n_{10} = the effective refractive index calculated by averaging the refractive indices of air and the nanocone structure as a function of the distance away from the bottom of the nanocone). As shown in Figure 5, we performed these Fresnel calculations for Au nanocone arrays and ZnO−Au nanocone arrays, and the simulated reflectivity measurements match closely to our reflectivity measurements over a wide spectral range. These calculations reveal that most of the observed decrease in reflectivity for the ZnO−Au nanocone arrays is due to the addition of a significant real refractive index component to the graded Au film (e.g., at 600 nm, n_{Au} = 0.24 + 3.10i, n_{ZnO} = 2.00 + 0i, and ZnO−Au is modeled using n_{ZnO-Au} = 2.00 + 3.10i). Details for the parameters used in the 11-phase Fresnel calculations are explained in the Supporting Information.

Even more striking results were obtained for the PEDOT nanocone array surfaces. Visually, we observed once again from the photograph shown in Figure 6c that the ZnO-PEDOT nanocone arrays were blacker than the PEDOT nanocone arrays. In Figure 6a, reflectivity measurements showed that, while the PEDOT nanocone arrays were less than 3% reflective (R < 3%) from 450 to 800 nm at θ = 8°, the ZnO−PEDOT nanocone arrays were more than an order of magnitude less reflective at R < 0.2% over the same spectral range. Furthermore, a comparison between the reflectivity measurements of ZnO electrodeposited on a planar PEDOT thin film surface (R < 5%) and the ZnO−PEDOT nanocone arrays (R < 0.2%) reveals that the periodicity of the nanocone arrays, as opposed to just the roughness created by the ZnO crystals, is critical in suppressing reflectivity. Since the reflectivity spectra for both the ZnO−Au and ZnO−PEDOT nanocone arrays are very similar, the mechanism for the suppressed reflectivity of the ZnO−PEDOT nanocone arrays must be similar and thus can also be explained by an enhancement in the graded interfacial complex refractive index and increased light scattering of the ZnO nanostructured surface. Finally, a very similar decrease in broadband reflectivity was also obtained for both ZnO−Au and ZnO−PEDOT nanocone arrays at higher angles of incidence (θ = 45° and θ = 67.5°), as shown in Figure 7. To the best of our knowledge, no one has fabricated surfaces with lower reflectivity than our broadband ultra-antireflective ZnO nanostructured surfaces.

■ CONCLUSIONS

We have demonstrated that electrodeposition of nanostructured ZnO films onto both FEP−Au and PEDOT periodic nanocone arrays creates excellent broadband antireflective surfaces that are less than 0.2% reflective over a large optical wavelength range of 475 to 800 nm. These surfaces are up to 10 times more antireflective than the nanocone arrays without the ZnO film. The nanostructured ZnO coating enhances (i) light scattering and (ii) the graded interfacial complex refractive index created by the Au or PEDOT nanocone array structures, which is responsible for broadband antireflectivity. The ZnO nanostructures created from this process also increase the

DOI: 10.1021/acs.jpcc.7b07503
J. Phys. Chem. C 2017, 121, 22377−22383

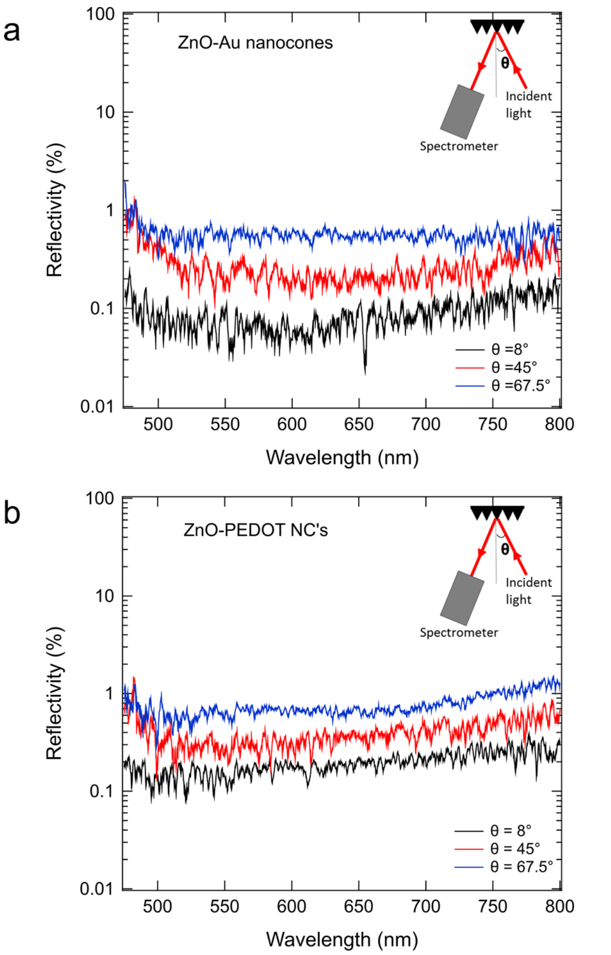

Figure 7. Reflectivity spectra for (a) ZnO−Au nanocone arrays and (b) ZnO−PEDOT nanocone arrays at various angles of incidence (θ), at 8° (black), 45° (red), and 67.5° (blue). The inserted schematic shows the optical setup used for reflectivity measurements.

surface area of the nanocone arrays, resulting in a higher surface reactivity for potential photocatalytic applications. As these ZnO-coated nanocone array surfaces are easy to fabricate over large surface areas on flexible substrates, they should be easily implemented in various potential applications such as highly antireflective self-cleaning surface coatings for displays and solar panels.

■ ASSOCIATED CONTENT

Supporting Information

The Supporting Information is available free of charge on the ACS Publications website at DOI: 10.1021/acs.jpcc.7b07503.

(i) Experimental details for the Fresnel calculations used to obtain the simulated %*R* measurements for nanocone arrays, (ii) electrochemical data of ZnO thin film electrodeposition, (iii) XRD and (iv) XPS spectra of ZnO-coated nanocone arrays, and (v) UV−vis spectra of relative MB concentrations under various photocatalytic conditions (PDF)

■ AUTHOR INFORMATION

Corresponding Author

*E-mail: rcorn@uci.edu.

ORCID

Han Wai Millie Fung: 0000-0003-0667-4113
Gabriel Loget: 0000-0003-4809-5013
Robert M. Corn: 0000-0002-4756-2161

Present Address

†Institut des Sciences Chimiques de Rennes, UMR 6226 CNRS, Université de Rennes 1, Campus de Beaulieu, 35042 Rennes Cedex, France.

Notes

The authors declare no competing financial interest.

■ ACKNOWLEDGMENTS

This work was supported by the National Science Foundation through grant CHE-1403506.

■ REFERENCES

(1) Chen, Y.; Xu, Z.; Gartia, M. R.; Whitlock, D.; Lian, Y.; Liu, G. L. Ultrahigh Throughput Silicon Nanomanufacturing by Simultaneous Reactive Ion Synthesis and Etching. *ACS Nano* **2011**, *5*, 8002−8012.

(2) He, J.; Gao, P.; Liao, M.; Yang, X.; Ying, Z.; Zhou, S.; Ye, J.; Cui, Y. Realization of 13.6% Efficiency on 20 um Thick Si/Organic Hybrid Heterojunction Solar Cells via Advanced Nanotexturing and Surface Recombination Suppression. *ACS Nano* **2015**, *9*, 6522−6531.

(3) Fujii, T.; Gao, Y.; Sharma, R.; Hu, E. L.; DenBaars, S. P.; Nakamura, S. Increase in the Extraction Efficiency of GaN-Based Light-Emitting Diodes via Surface Roughening. *Appl. Phys. Lett.* **2004**, *84*, 855−857.

(4) Araki, S.; Nakamura, K.; Kobayashi, K.; Tsuboi, A.; Kobayashi, N. Electrochemical Optical-Modulation Device with Reversible Transformation Between Transparent, Mirror, and Black. *Adv. Mater.* **2012**, *24*, OP122−OP126.

(5) Wu, J. J.; Liu, S. C. Low-Temperature Growth of Well-Aligned ZnO Nanorods by Chemical Vapor Deposition. *Adv. Mater.* **2002**, *14*, 215−217.

(6) Peiro, A. M.; Ravirajan, P.; Govender, K.; Boyle, D. S.; O'Brien, P.; Bradley, D. D. C.; Nelson, J.; Durrant, J. R. Hybrid Polymer/Metal Oxide Solar Cells Based on ZnO Columnar Structures. *J. Mater. Chem.* **2006**, *16*, 2088−2096.

(7) Montenegro, D. N.; Souissi, A.; Martinez-Tomas, C.; Munoz-Sanjose, V. Sallet, V. Morphology Transitions in ZnO Nanorods Grown by MOCVD. *J. Cryst. Growth* **2012**, *359*, 122−128.

(8) Wahab, R.; Ansari, S. G.; Kim, Y. S.; Seo, H. K.; Kim, G. S.; Khang, G.; Shin, H.-S. Low Temperature Solution Synthesis and Characterization of ZnO Nano-Flowers. *Mater. Res. Bull.* **2007**, *42*, 1640−1648.

(9) Illy, B. N.; Cruickshank, A. C.; Schumann, S.; Da Campo, R.; Jones, T. S.; Heutz, S.; McLachlan, M. A.; McComb, D. W.; Riley, D. J.; Ryan, M. P. Electrodeposition of ZnO Layers for Photovoltaic Application: Controlling Film Thickness and Orientation. *J. Mater. Chem.* **2011**, *21*, 12949−12957.

(10) Sun, S.; Jiao, S.; Zhang, K.; Wang, D.; Gao, S.; Li, H.; Wang, J.; Yu, Q.; Guo, F.; Zhao, L. Nucleation Effect and Growth Mechanism of ZnO Nanostructures by Electrodeposition from Aqueous Zinc Nitrate Baths. *J. Cryst. Growth* **2012**, *359*, 15−19.

(11) Klochko, N. P.; Khrypunov, G. S.; Myagchenko, Y. O.; Melnychuk, E. E.; Kopach, V. R.; Klepikova, K. S.; Lyubov, V. M.; Kopach, A. V. Electrodeposited Zinc Oxide Arrays with the Moth-Eye Effect. *Semiconductors* **2014**, *48*, 531−537.

(12) Tsui, K.; Lin, Q.; Chou, H.; Zhang, Q.; Fu, H.; Qi, P. Low-Cost, Flexible, and Self-Cleaning 3D Nanocone Anti-Reflection Films for High-Efficiency Photovoltaics. *Adv. Mater.* **2014**, *26*, 2805−2811.

(13) Leem, J. W.; Kim, S.; Lee, S. H.; Rogers, J. A.; Kim, E.; Yu, J. S. Efficiency Enhancement of Organic Solar Cells Using Hydrophobic Antireflective Inverted Moth-Eye Nanopatterned PDMS Film. *Adv. Energy Mater.* **2014**, *4*, 1−7.

(14) Wang, Y.; Lu, N.; Xu, H.; Shi, G.; Xu, M.; Lin, X.; Li, H.; Wang, W.; Qi, D.; Lu, Y.; et al. Biomimetic Corrugated Silicon Nanocone

Arrays for Self-Cleaning Antireflection Coatings. *Nano Res.* **2010**, *3*, 520−527.
(15) Garnett, E.; Yang, P. Ordered Arrays of Dual-Diameter Nanopillars for Maximized Optical Absorption. *Nano Lett.* **2010**, *10*, 1082−1087.
(16) Wilson, S. J.; Hutley, M. C. The Optical Properties of 'Moth Eye' Antireflection Surfaces. *Opt. Acta* **1982**, *29*, 993−1009.
(17) Toma, M.; Loget, G.; Corn, R. M. Fabrication of Broadband Antireflective Plasmonic Gold Nanocone Arrays on Flexible Polymer Films. *Nano Lett.* **2013**, *13*, 6164−6169.
(18) So, S.; Fung, H. W. M.; Kartub, K.; Maley, A. M.; Corn, R. M. Fabrication of PEDOT Nanocone Arrays with Electrochemically Modulated Broadband Antireflective Properties. *J. Phys. Chem. Lett.* **2017**, *8*, 576−579.
(19) Li, Y.; Zhang, J.; Zhu, S.; Dong, H.; Jia, F.; Wang, Z.; Sun, Z.; Zhang, L.; Li, Y.; Li, H.; et al. Biomimetic Surfaces for High-Performance Optics. *Adv. Mater.* **2009**, *21*, 4731−4734.
(20) Busse, L. E.; Florea, C. M.; Frantz, J. A.; Shaw, L. B.; Aggarwal, I. D.; Poutous, M. K.; Joshi, R.; Sanghera, J. S. Anti-Reflective Surface Structures for Spinel Ceramics and Fused Silica Windows, Lenses and Optical Fibers. *Opt. Mater. Express* **2014**, *4*, 2504−2515.
(21) Nuijs, A. M.; Horikx, J. J. Diffraction and Scattering at Antiglare Structures for Display Devices. *Appl. Opt.* **1994**, *33*, 4058−4068.
(22) Tulli, D.; Hart, S. D.; Mazumder, P.; Carrilero, A.; Tian, L.; Koch, K. W.; Yongsunthon, R.; Piech, G. A.; Pruneri, V. Monolithically Integrated Micro- and Nanostructured Glass Surface with Antiglare, Antireflection, and Superhydrophobic Properties. *ACS Appl. Mater. Interfaces* **2014**, *6*, 11198−11203.
(23) Shen, W.; Li, Z.; Wang, H.; Liu, Y.; Guo, Q.; Zhang, Y. Photocatalytic Degradation for Methylene Blue using Zinc Oxide Prepared by Codeposition and Sol-Gel Methods. *J. Hazard. Mater.* **2008**, *152*, 172−175.
(24) Jang, Y. J.; Simer, C.; Ohm, T. Comparison of Zinc Oxide Nanoparticles and its Nano-Crystalline Particles on the Photocatalytic Degradation of Methylene Blue. *Mater. Res. Bull.* **2006**, *41*, 67−77.
(25) Voss, T.; Svacha, G. T.; Mazur, E.; Konjhodzic, D.; Marlow, F. High Order Waveguide Modes in ZnO Nanowires. *Nano Lett.* **2007**, *7*, 3675−3680.
(26) Kim, S. K.; Song, K. D.; Kempa, T. J.; Day, R. W.; Lieber, C. M.; Park, H. G. Design of Nanowire Optical Cavities as Efficient Photon Absorbers. *ACS Nano* **2014**, *8*, 3707−3714.
(27) Chang, Y.-M.; Lin, M.-L.; Lai, T.-Y.; Chen, C.-H.; Lee, H.-Y.; Lin, C.-M.; Wu, Y.-C. S.; Lin, Y.-F.; Juang, J.-Y. Broadband Omnidirectional Light Trapping in Gold-Decorated ZnO Nanopillar Arrays. *ACS Appl. Mater. Interfaces* **2017**, *9*, 11985−11992.
(28) Tian, Y.; Hu, C.; Xiong, Y.; Wan, B.; Xia, C.; He, X.; Liu, H. ZnO Pyramidal Arrays: Novel Functionality in Antireflection. *J. Phys. Chem. C* **2010**, *114*, 10265−10269.
(29) Robak, E.; Kotkowiak, M.; Drozdowski, H. Nanostructured Zinc Oxide Systems with Gold Nanoparticle Pattern for Efficient Light Trapping. *J. Phys. D: Appl. Phys.* **2016**, *49*, 045104.
(30) Xu, S.; Adiga, N.; Ba, S.; Dasgupta, T.; Wu, C. F. J.; Wang, Z. L. Optimizing and Improving the Growth Quality of ZnO Nanowire Arrays Guided by Statistical Design of Experiments. *ACS Nano* **2009**, *3*, 1803−1812.
(31) Jheng, B.-T.; Liu, P.-T.; Wang, M.-C.; Wu, M.-C. Effects of ZnO-Nanostructure Antireflection Coatings on Sulfurization-Free Cu_2ZnSnS_4 Absorber Deposited by Single-Step Co-Sputtering Process. *Appl. Phys. Lett.* **2013**, *103*, 052904.
(32) Bond, W. L. Measurement of the Refractive Indices of Several Crystals. *J. Appl. Phys.* **1965**, *36*, 1674−1677.

DOI: 10.1021/acs.jpcc.7b07503
J. Phys. Chem. C 2017, 121, 22377−22383